Charles University in Prague
Faculty of Mathematics and Physics

**BACHELOR THESIS**

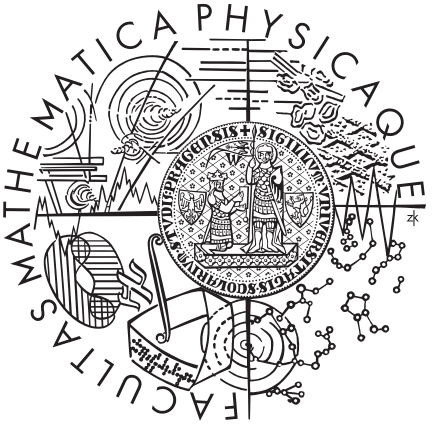


Jan Sopoušek

# Analysis of Tunnelling Current Fluctuations in STM

Department of Surface and Plasma Science

Supervisor of the bachelor thesis: doc. RNDr. Ivan Ošťádal, CSc.

Study programme: Physics

Prague 2014

I would like to thank my supervisor doc. RNDr. Ivan Ošťádal, CSc. for his advice on the topic, Mgr. Filip Rozbořil for his help with measuring by STM and finally my other collegues from Thin Films Group at MFF.

I declare that I carried out this bachelor thesis independently, and only with the cited sources, literature and other professional sources.

I understand that my work relates to the rights and obligations under the Act No. 121/2000 Coll., the Copyright Act, as amended, in particular the fact that the Charles University in Prague has the right to conclude a license agreement on the use of this work as a school work pursuant to Section 60 paragraph 1 of the Copyright Act.

In ..... date .....  signature of the author

Název práce: Analýza fluktuací tunelového proudu v STM

Autor: Jan Sopoušek

Katedra: Katedra fyziky povrchů a plazmatu

Vedoucí bakalářské práce: doc. RNDr. Ivan Ošťádal, CSc., KFPP

Abstrakt: Práce se zabývá analýzou fluktuací tunelového proudu v skenovací tunelovací mikroskopii (STM). Je studována dynamika atomů Sn na povrchu Si (111) $7 \times 7$ za použití časového záznamu tunelového proudu. Z jeho zpracování jsou určeny doby, po které atom Sn setrvává v různých oblastech půlcel povrchové rekonstrukce. Dále jsou studovány jednotlivé modelové typy rušení tunelového proudu, které mají vliv na přesnost provedeného experimentu.

Klíčová slova: STM, fluktuace, Si (111) $7 \times 7$

Title: Analysis of Tunnelling Current Fluctuations in STM

Author: Jan Sopoušek

Department: Department of Surface and Plasma Science

Supervisor: doc. RNDr. Ivan Ošťádal, CSc., KFPP

Abstract: The thesis deals with analysis of fluctuations of the tunnelling current in scanning tunnelling microscopy (STM). The dynamics of Sn atoms on the surface Si (111) $7 \times 7$ is studied by means of time records of the tunnelling current. The records provided characteristic times of Sn adatom staying in various areas of half unit cells of the surface reconstructions are analysed. The model types of the tunnelling current interference, which influence the measurement accuracy, are also studied.

Keywords: STM, fluctuation, Si (111) $7 \times 7$

# Contents

# Introduction

In modern world we use electronic devices every day. With requests of higher capabilities and speed of the devices technology industry have to improve manufacturing processes. For such processes we need to understand deeper basic mechanisms of the processes. One of the "know-how" which is essential for making epitaxial layers which is the only technology how to make pure crystals with material structures that can not be done by any other conventional method is the knowledge of parameters of surface diffusion mechanism.

One of the techniques how to study surface diffusion is scanning tunnelling microscopy (STM) in ultra-high vacuum which allows atomic resolution. This thesis deals with analysis of fluctuations of tunnelling current in STM. The surface diffusion of tin on silicon surface (111) $7 \times 7$ is studied in the thesis. The research is done in microscopic view which the STM microscopy can offer. The diffusion can be also studied by another techniques such as some spectroscopy techniques, electron diffraction etc. but none of them can bring microscopic view.

The tasks of the thesis are:

- Mastering the technique of measurement by STM.
- Understanding the basics of time series analysis.
- Generation of the model examples of controlled parasitic fluctuations of the tunnelling current and their characterisation.
- Preparation of the Si(111) $7 \times 7$ surface and deposition of the very small amount of metal (Sn) and display of the metal monomers on the surface at room and low temperatures

The thesis is part of the research of Thin Films Group of Department of Electronics and Vacuum Physics, MFF, UK in Prague. It follows previous research of silver on silicon surface and other atoms on it.

The text of the thesis is divided into several chapters. In the first chapter I sum up basic theory needed to understand the issue. The second chapter is about methodology of acquisition and evaluation of experimental data. The third section contains description of the used machine and experimental set-up. Finally in the last chapter there is a summary of the elaborated experiments.

# I. Theoretical Background

In this chapter I briefly introduce basics of physical theory of topics which are important in my research. I apprise reader with scanning tunnelling microscopy, quantum tunnelling phenomenon, noise of tunnelling current and finally surface Si (111) $7 \times 7$ and difussion of an adsorbed atom on it.

## I.1 Scanning Tunnelling Microscopy

A scanning tunnelling microscopy is microscopy imaging technique which uses tunnelling current (see section I.2). The tunnelling current is measured between

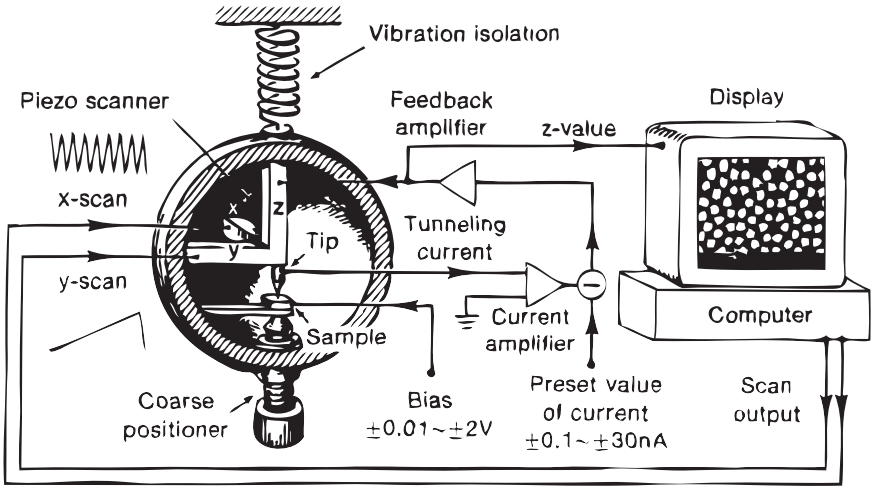


**Figure I.1:** Schematic diagram of STM[4]

the scanning tip and the surface of the sample. The current is held on a given level by using a regulator and by moving of the tip further or closer to the surface. We can see the surface by scanning over and measuring the z-position of the tip.

STM operates usually at ultra-high vacuum which allows clear surfaces necessary to resolve surface atoms. Atomic resolution is given by the exponential law of tunnelling current with changing distance of the tip from the sample. Thus the tunnelling current flows only in a very small area. Because the tunnelling current is, apart from probability of tunnelling, proportional to the local electron density it brings even information about the electron structure.

### I.1.1 Modes of Operation

The tip of the microscope is held in a position by piezoelectric actuators. The scanning can be performed in different modes. The first one which was also used in my research is the constant current mode during which the z-position of the

tip is adjusted by a feedback loop. The z-position carries the information about sample topography.

Another mode is the constant height mode during which the z-position is held and the tunnelling current is measured. This mode can be used only on flat surfaces because the tip could crash into the sample if there is a high elevation step. An advantage of this mode is that higher scan speed can be reached.

We can also perform spectroscopic measurement when we hold the z-position constant, apply different bias voltage and measure I-V characteristics, which reflect density of states at the tip position. Finally the microscope can be also used to manipulate with atoms on the surface by special procedures when the voltage bias on the tip and the z-position are being changed on purpose.

## I.2 Tunnelling Current

Quantum tunnelling of the electron is the phenomenon which occurs in nanometre length scale. The electron can be described by a wave function and therefore there is non-zero probability to go through a potential barrier higher than the energy of the electron.

### I.2.1 WKB Approximation of Tunnelling Junction

Let an electron be described by an one-dimensional wave function $\phi(x)$ and the field be described by potential energy $V(x)$. $\phi(x)$ has to satisfy the time independent Schrödinger equation:

$$-\frac{\hbar^2}{2m_e}\Delta\phi(x) = (E - V(x))\phi(x) \tag{I.1}$$

Where $\hbar$ is the reduced Planck's constant, $m_e$ is mass of the electron and $E$ is its energy. We suppose that there are $x_1$, $x_2$ such as:

$$\begin{aligned} V(x) < E \quad & x \in (-\infty, x_1) \cup (x_2, -\infty) \\ V(x) > E \quad & x \in (x_1, x_2) \end{aligned} \tag{I.2}$$

$(-\infty, x_1) \cup (x_2, -\infty)$ corresponds to the classically allowed region and $(x_1, x_2)$ to the forbidden region (figure I.2). By using WKB approximation we can solve the Schrödinger equation I.1 and get the transmission coefficient of tunnelling through the barrier[2]:

$$T_{WKB} = e^{-\frac{2}{\hbar}\int_{x_1}^{x_2}\sqrt{2m_e(V(x)-E)}dx} \tag{I.3}$$

which corresponds to the probability of electron tunnelling. The tunnelling current $I$ is proportional to the probability of electron tunnelling. For a squared potential energy:

$$\begin{aligned} V(x) = 0 \quad & x \in (-\infty, x_1) \cup (x_2, -\infty) \\ V(x) = V > E \quad & x \in (x_1, x_2) \end{aligned} \tag{I.4}$$

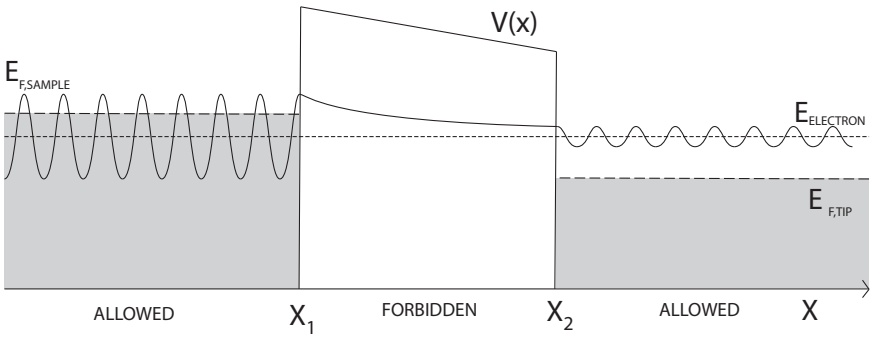


**Figure I.2:** Example of the tunnelling junction

We obtain:

$$I \approx T_{WKB} = e^{-\frac{2}{\hbar}\sqrt{2m_e(V-E)}\Delta x} \tag{I.5}$$

Where $\Delta x = x_2 - x_1$ is the width of the barrier. Results are counted for a planar case but it brings out important dependence of tunnelling current on width of the tunnelling barrier. The tunnelling current is exponentially decreasing with increasing barrier width thus it can occur only for a very thin barrier which is in order of tens of angstrom.

### I.2.2 Bardeen's approach

The electron tunnelling phenomenon in STM can be described by Bardeen's approach which is based on the time dependent perturbation theory. The Bardeen's approach takes into account densities of state of the tip and the sample and thus describe better the real situation.

According to the Fermi's Golden Rule the probability of an electron tunnelling from state $\phi$ with energy $E_\phi$ to state $\psi$ with $E_\psi$ is given by[4]:

$$W_{\phi\psi} = \frac{2\pi}{\hbar}|M_{\phi\psi}|^2\delta(E_\psi - E_\phi) \tag{I.6}$$

Where $\delta$ is a delta function and matrix elements $M_{\phi\psi}$ are given by:

$$M_{\phi\psi} = -\frac{\hbar^2}{2m}\int_S(\psi^*\nabla\phi - \phi\nabla\psi^*)dS \tag{I.7}$$

Where it is integrated at a surface $S$ which lies between the tip and the sample.

By integrating over all states in the sample and the tip and considering the occupation probabilities we obtain the final equation of the tunnelling current:

$$\begin{aligned} I = \frac{4\pi e}{\hbar}\int_{-\infty}^{\infty}(f(E_F - eV + \epsilon) - f(E_F + \epsilon)) \cdot \\ \cdot\rho_S(E_F - eV + \epsilon)\rho_T(E_F + \epsilon)|M|^2\mathrm{d}\epsilon \end{aligned} \tag{I.8}$$

Where $f$ is the Fermi distribution, $E_F$ Fermi energy, $V$ voltage bias and $\rho_S, \rho_T$ densities of states of the sample and the tip.

If we know the density of states of the tip, it is possible to determine the density of states of the sample by measuring the current-voltage characteristic from the equation I.8.

## I.3 Electrical Noise

The thesis deals with measuring of mobility of atoms on the sample surface which can be determined by measuring counting of occurrence of atoms under the tip. The tunnelling current changes its level according to the atom presence under the tip. Because the amount of the current is in the order of tens to hundreds of picoampere it is critical to distinguish between a noise and a desired signal. The most common possible types of noise in STM measuring are shot noise, flicker noise and interference of the surrounding.

### I.3.1 Shot Noise

Electrical current is not continuous but it flows by electrons. The probability of passing of $n$ electrons during time $\Delta t$ is given by the Poisson distribution[1]. The mean value of the measured current is equal to:

$$I = \bar{i} = \frac{e\bar{n}}{\Delta t} \tag{I.9}$$

Where $e$ is the charge of an electron and $\bar{n}$ is the mean value of the Poisson distribution. The mean square value of the current fluctuation is given by:

$$\overline{(i-\bar{i})^2} = \left(\frac{e}{\Delta t}\right)^2 \overline{(n-\bar{n})^2} = \left(\frac{e}{\Delta t}\right)^2 \bar{n} \tag{I.10}$$

By combination of equations I.9 and I.10 we obtain:

$$\overline{(i-\bar{i})^2} = \frac{e}{\Delta t} I \tag{I.11}$$

$\Delta t$ is the duration of the shortest measured time and is in the order of the reciprocal bandwidth $\Delta f$:

$$\overline{(i-\bar{i})^2} = 2eI\Delta f \tag{I.12}$$

The number 2 is because we consider only positive frequencies. Spectral noise density $p(f)$ is thus frequency independent:

$$p(f) = 2eI \tag{I.13}$$

From equation I.12 it would seem that the current noise is infinite. However, in real system the bandwidth is limited by a maximal frequency.

### I.3.2 Flicker Noise

In electronic devices there is so called "1/f" noise. The spectral noise density can be expressed as[1]:

$$p(f) = \text{const}\frac{I^\beta}{f^\alpha} \tag{I.14}$$

Where $\alpha \simeq 1$ and $\beta \simeq 2$. The physical origin of this noise in STM is not yet clearly identified despite a lot of research on the topic have been done.

Some of the explanations are linked to relaxation processes[21][18]. When the surface is not clear, flicker noise can be explained by diffusion[11].

### I.3.3 Mechanical Noise

Mechanical noise of tunnelling current often occur in the inadequately soundproof room where the STM device is located. Also some parts of the measuring apparatus such as the tip, the sample, mechanics etc. could have some resonance frequencies.

Let's evaluate basic harmonic wave of the distance $z$ (sample to tip):

$$z = z_0 + A \sin 2\pi f t \tag{I.15}$$

Where $f$ is its frequency, $z_0$ is the equilibrium distance and $A$ is the amplitude of the mechanic wave. The tunnelling current then fluctuates as:

$$i = Ce^{A' \sin 2\pi f t} \tag{I.16}$$

Where $C$ is a constant. If we had estimated spectral noise density we would have seen peaks with frequencies $nf$ where $n$ is an integer. Unfortunately the Fourier transform can not be calculated analytically.

In figure I.3 I calculated the spectral noise density for the fluctuation in z-axis by same procedure as I used in the experiments (see below in section II.4) with frequency of oscillations 1 kHz, sampling frequency 20 kHz and using $2^{18}$ points long record. As it was expected the spectrum contains the most intense fundamental frequency and also overtones which are fading with higher frequencies.

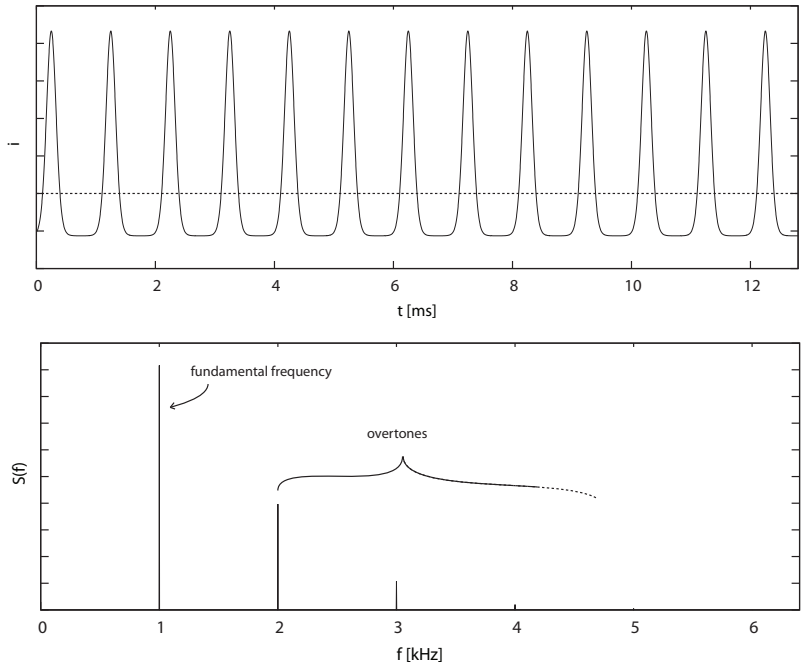


**Figure I.3:** Mechanical noise of the tunnelling current with constant C=1, A=4 and its spectral noise density

### I.3.4 Electrical Interference

Because the tunnelling current is only about several hundreds of pA the STM measurement is highly sensitive of electrical interference. Electrical interference

can be caused by electromagnetic waves in air but more often, and also because vacuum chamber of STM acts as a Faraday cage, is caused by fluctuations of electric network. Electrical interference is characterised by peaks in spectral noise density. The most intense sources are switched-mode power supplies. Electrical interference of electric network can be partly eliminated by proper connection of shielding wires to the STM apparatus. Basically, there should not be closed wire loops where electric voltage can be induced.

### I.3.5 Other Types of Noise

In STM measurement there can also occur other types of noise such as thermal noise of materials which changes its resistance, burst noise caused by bad contact of the electronic parts, etc. Those types are not mostly so intense in STM measurement and can be neglected. The thermal fluctuation of voltage $v$ is given by formula[9]:

$$\overline{(v-\bar{v})^2} = 4k_B T R \Delta f \tag{I.17}$$

Where $k_B$ is Boltzmann's constant and $T$ temperature. By using Ohm's law we obtain the power noise density of the current:

$$p(f) = 4k_B T \frac{I}{V} \tag{I.18}$$

If we compare it (laboratory temperature, units of volts) with shot noise (equation I.13), we get that it is about fifty times smaller.

## I.4 Silicon (111) $7 \times 7$ Reconstruction

Major part of the thesis research deals with the study of adsorbed atoms on Si surface (111) $7 \times 7$. Let's shortly introduce the surface. Silicon has a diamond lattice structure. The surface with Miller indices (111) made by breaking bonds is not thermodynamically stable. The surface can be changed by heating in ultra-high vacuum into more stable $7 \times 7$ reconstruction. The reconstruction can be described by a "Dimer-Adatom-Stacking fault" (DAS) model (Figure I.5).

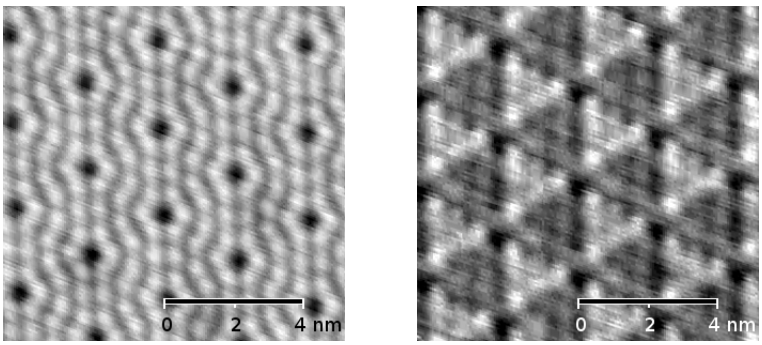


a. unoccupied electron states b. occupied electron states

**Figure I.4:** STM scan of Si (111) $7 \times 7$ reconstruction at 2 V

Basically, it is made by primitive cells 7 times bigger than the primitive cell of the ideal (111) surface. The cell can be divided to two non-equivalent half-cells which are called as unfaulted and faulted according to the position of the 3rd bilayer. The reconstructed surface is made by the changed first layer with dimers on borders of the half cells and twelve adatoms on it. In Figure I.4 there is the measured reconstructed surface by STM.

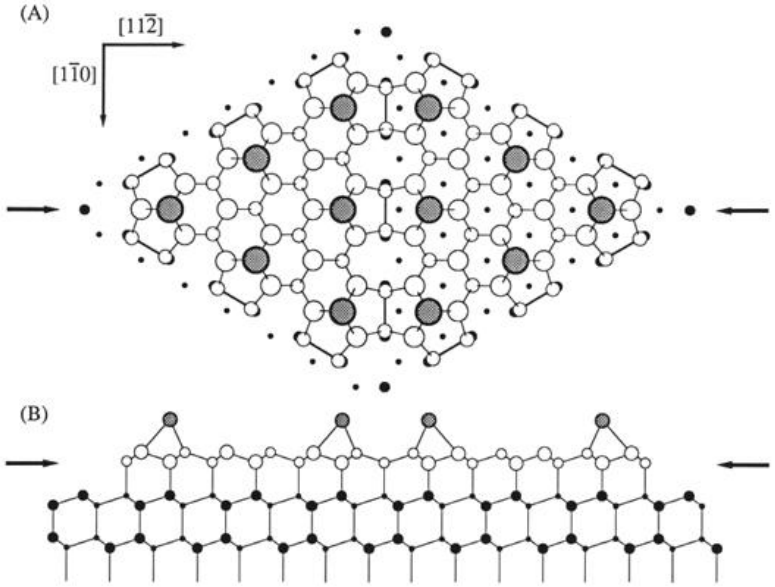


**Figure I.5:** Si (111) $7 \times 7$ reconstruction (A) Plan view. The grey disks denote adatoms, the middle sized bright disks denote rest atoms, and a pair of small disks connected by thick lines denote a dimer pair. The right and left triangles are called unfaulted and faulted stacking halves, respectively. (B) Cross section at the long diagonal[17]

## I.5 Adsorbed Atoms on Si (111) $7 \times 7$ Surface

One of the subjects of the research is the study of diffusion of adsorbed atoms on Si (111) $7 \times 7$ surface (Figure I.4). This surface has special properties because it is formed of elementary cells which have such potential-energy profile of adsorbed atoms that keeps them almost within the half-cell (Figure I.6). Thus the atoms move only among several adsorption positions.
Let's study the kinetics of the movement of the adsorbed atom. The movement of the atoms on the surface can be treated as a chemical reaction, the reaction path is thus the path of moving of the atom on the surface. According to the transition state theory the atom can move from the I. position to the II. position with the transition rate[22]:

$$k = \frac{k_B T}{h} \frac{Q^{\#}}{Q_{I.}} e^{-\frac{E_A}{k_B T}} \tag{I.19}$$

Where $k_B$ is Boltzmann constant, $h$ Planck's constant, $T$ temperature, $Q^{\#}$ the partition function of the transition state, $Q_{I.}$ the partition function of the I. state and $E_A$ is activation energy.

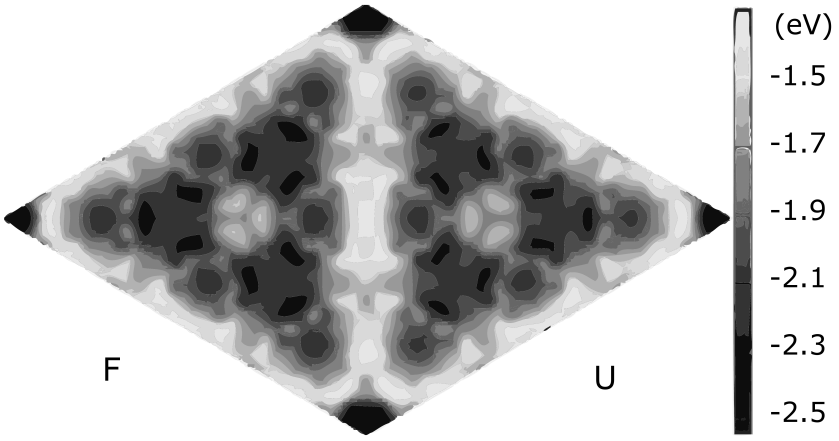


**Figure I.6:** Potential energy profile of Ag atom on Si (111) $7 \times 7$ cell[24]

The mean lifetime of the I. adsorption position corresponding to the reaction path is then the reciprocal value of the transition rate:

$$\tau = \frac{h}{k_B T} \frac{Q_{I.}}{Q^{\#}} e^{\frac{E_A}{k_B T}} \tag{I.20}$$

By measuring of the temperature dependence of the mean lifetime we can determine the activation energy of the barrier. In some positions there can be more different reaction paths which the atoms can go through. If mean lifetimes are distinguishable enough, we can determine them both.

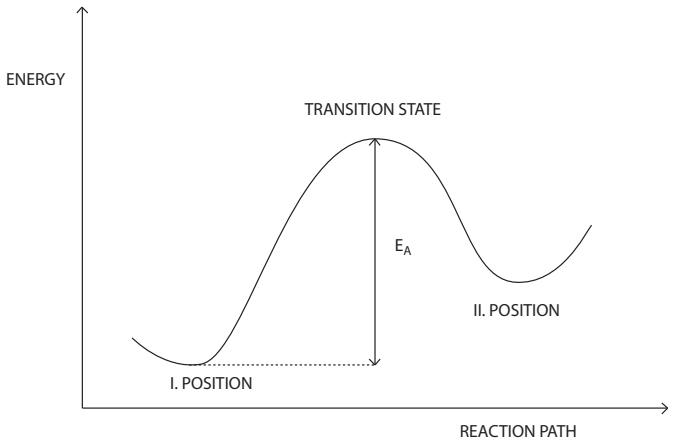


**Figure I.7:** Illustration of the reaction path

# II. Methodology

## II.1 Sample Preparation

As it was stated, fluctuation of atoms of Tin on Si (111) $7 \times 7$ surface is studied. Before the measurement itself we need to modify the surface to have optimal properties. Usually, there is an oxide layer on silicon surface so after putting the sample to the vacuum chamber and reaching appropriate pressure the sample is heated by current flow and kept at high temperature (about 600° C) for several hours at which the sample is still protected by its oxide layer but the other absorbed gases (water etc.) desorb away. After about 15 hours the sample temperature is quickly increased to approximately 1200° C and the oxide layer is dismissed. This is called sample flashing. The temperature is slowly lowered to 900° C (rampdown) to make the $7 \times 7$ reconstruction. The sample is then cooled down to room temperature. After this process we obtain clean Si surface with $7 \times 7$ reconstruction.

The tin evaporator is used for applying tin gas. The evaporator consists of the tantalum tube with tin and tungsten spiral wire. The spiral is heated to 1300° C (sufficient vapour pressure) by Joule resistance heating and beam of evaporated tin atoms is focused onto the sample. The deposition time is controlled by opening and closing the shutter of the evaporation source.

## II.2 Tip Enhancement

The STM tip is very sensitive to any disorder on the sample or the misconfiguration of atoms at the very tip. It sometimes happens during scanning that the tip has too big a radius, there is a configuration of atoms which are oscillating or the tip is multiple. If that occurs, the resolution of the image highly decreases. Thus we need to enhance the tip. There exist several techniques to do so.

The basic one is increasing the voltage bias at the tip for several milliseconds. The procedure is the same as the acquisition of current-voltage characteristics with start and final voltage set to about 4 V. High bias can, with low probability, readjust atom configuration at the very tip or drop them off the tip.

The second technique is the high current treatment when the current level from the tip to the sample is set to about 15 nA or more (we usually scan by 0.2-0.3 nA) for several seconds. Because the current flows in very small area, atoms on the tip tend to locate along the flowing current and thus sharpen the tip.

Finally, the third welding technique is probably the most effective but long-term because we need to get the microscope off the contact with the scanned sample and move over a tungsten strip. The tip is weld to the thermionic tungsten strip by increased voltage and current and after that it is pulled off the strip. The tip should be really sharp with metal properties.

## II.3 STM Data Acquisition

The scanning process starts with approaching of the tip to the sample. The tip is manually moved closer to the sample and then with the current regulator switched on it is auto approached to the sample. The regulator disables crashing of the tip into the sample.

After the approach, the scan process can begin. The slope of the sample is corrected by manually setting the angle of the tip. The tip position is controlled by changing voltage on the piezoelectric ceramics in axes x,y and also z. Mostly, the thermal drift has to be equilibrated during several first scans. If the thermal drift is stable, it can be also corrected by setting constant drifting velocity of the tip so the tip moves along the sample.

The constant current mode is used for the measurement. The scanning on Si surface is done with 2 V bias and 0.2 or 0.3 nA. The PID regulator is used to hold the current level but only integral parameter of the regulator is set. Proportional or derivative parameters can not be used because it could cause the tip-to-sample impact.

## II.4 Spectral Analysis

In this section I will shortly introduce the used algorithms of data processing. First of all in every measurement we acquire data series of the tunnelling current $i(t_k)$ in times $t_k$ where $k = 0..N$ with the sampling period $\tau = t_{k+1} - t_k$. According to the sampling theorem[20] the maximal (critical) frequency is:

$$f_s = \frac{1}{2\tau}$$

On the other hand the lowest non-zero frequency is equal to:

$$f_0 = \frac{1}{\tau N}$$

Thus if we want to study long-term phenomena we have to increase measuring time $\tau N$.

For characterization of the time signal I use the spectral noise density which is related to mean square value of the current by the equation:

$$\overline{(i)^2} = \int_0^{f_{max}} p(f)df \tag{II.1}$$

Where $f_{max}$ is the maximal frequency which is limited by the amplifier.

In the thesis I analyse two types of signals: deterministic and stationary stochastic signals. Each of them is processed differently.

### II.4.1 Deterministic Signals

A deterministic signal is the signal which can be predicted by a mathematical model. If the signal is continuous the spectral noise density can be determined

precisely, however, because of signal sampling, we can only use discrete approximation. Let's, in continuous analysis, have signal $x_T(t)$:

$$x_T(t) = \begin{cases} x(t) & \text{if } 0 < t < T \\ 0 & \text{otherwise} \end{cases} \tag{II.2}$$

Such function guarantee the finiteness of the integral of $\int_{-\infty}^{\infty} |x_T(t)|dt$ needed for Fourier transform. The Fourier transform is then given by:

$$F_T(f) = \int_{-\infty}^{\infty} x_T(t) e^{-j2\pi ft} dt \tag{II.3}$$

Where $j$ is an imaginary unit.
Because of the Parseval equality:

$$\int_{-\infty}^{\infty} x_T^2(t)dt = \int_{-\infty}^{\infty} |F_T(f)|^2 df \tag{II.4}$$

The spectral noise density can be counted as:

$$p(f) = \lim_{T\to\infty} \frac{2}{T} |F_T(f)|^2 \tag{II.5}$$

The factor 2 is introduced because we consider only $f > 0$.

In the experiment the discrete time series has to be analysed. The analogous discrete version can be used if the sampling theorem is satisfied (sampling frequency has to be twice higher than maximal frequency in the spectrum). I count Fourier transform of signal series $i(t_k)$ by the Cooley–Tukey FFT algorithm:

$$F(f_n) = \tau \sum_{k=0}^{N-1} i(t_k) e^{-\frac{j2\pi nk}{N}} \tag{II.6}$$

And then the spectral noise density by the equation:

$$p(f_n) = \frac{2}{\tau N} |F(f_n)|^2 \tag{II.7}$$

### II.4.2 Stochastic Signals

A stochastic stationary signal has to be treated differently in general because the limit of Fourier transforms as duration of measurement goes to infinity does not have to exist at all. Thus the autocorrelation function of signal $f(t)$ is used:

$$A(\tau) = \int_{-\infty}^{\infty} f(t) f(\tau - t) dt \tag{II.8}$$

And the spectral noise density of the signal is then Fourier transform of the autocorrelation function:

$$p(f) = \int_{-\infty}^{\infty} A(\tau) e^{-j2\pi ft} dt \tag{II.9}$$

Though if we have discrete samples and limited measuring time, the spectral noise density can be counted as deterministic (it is faster to process) and the

autocorrelation function can be counted as the inverse Fourier transform of the spectral noise density.

In reality we have a two-level fluctuation signal and we need to evaluate the mean lifetime. To do so we can use the sequence above but because measured data is often too short for that type of analysis I use different method of processing.

At first I cut off high frequencies from the signal by setting the amplitudes at those frequencies to zero after Fourier transform. Then I transform it back and get the signal of the current with no high frequencies. Then the auto tresholding algorithms is applied to recognise the high and the low levels of the current. The Otsu's method is used. The time series $i(t_n)$ is divided into two parts $\{i(t_{j_1}), i(t_{j_2}), ...i(t_{j_n}),\}$ and $\{i(t_{k_1}), i(t_{k_2}), ...i(t_{k_m}),\}$ Then the mean value of the current is calculated for each part and the whole set:

$$\begin{aligned} \mu_0 &= \frac{1}{n}\sum_{l=1}^{n} i(t_{j_l}) \\ \mu_1 &= \frac{1}{m}\sum_{l=1}^{m} i(t_{k_l}) \\ \mu &= \frac{1}{N}\sum_{l=1}^{N} i(t_l) \end{aligned} \tag{II.10}$$

Then quantities $\omega_{0,1}$ are calculated:

$$\begin{aligned} \omega_0 &= \frac{1}{n}\sum_{l=1}^{n}(i(t_{j_l}) - \mu_0)^2 \\ \omega_1 &= \frac{1}{m}\sum_{l=1}^{m}(i(t_{k_l}) - \mu_1)^2 \end{aligned} \tag{II.11}$$

By minimisation of the expression:

$$\omega_0(\mu_0 - \mu) + \omega_1(\mu_1 - \mu) \tag{II.12}$$

over all arrangements we get appropriate assignment to the high and the low levels of the current.

When we have divided the time series of the current into separated levels we can count cumulative distribution $P(x < t)$ of duration of the Sn staying in high level of the current. For Poisson process the probability that the duration is less than $t$ should have functional characteristic:

$$P(x < t) = 1 - e^{-\frac{t}{\tau}} \tag{II.13}$$

By fitting this function we obtain mean lifetime $\tau$. The mean lifetime is thus the mean time when the Sn atom stays in the adsorption position.

## II.5 Image Processing

Scanned images are post-processed in programme Gwydion. Raw data obtained from STM consists of x,y and z position of the tip on the sample. Because we never eliminate misalignment absolutely, the polynomial background is subtracted from

the image. Then the median row centring filter is applied. We also need to determine positions of a measurement of tunnelling current time series in the half-cell of Si (111). For that purpose I manually measured the corner holes of the half-cell (dark points in unoccupied states scan) in programme ImageJ. Then I use the algorithm for triangulation. Steps of the triangulation algorithm are:

- Make an array A with every possible edge between two vertices
- Sort the array A by edge length using quick sort algorithm.
- Make an array B where we put the chosen edges which make the triangulation graph.
- For each edge in array A starting with the shortest one check if the edge is not crossing any edge in B and if it is not then move the edge to the array B
- Finally, get over array B and make a list of triangles .

With this algorithm we obtain triangulation with minimal lengths of edges so if the pattern is made by equilateral triangles, it works really well. Unfortunately, some of the scanned images are deformed. Thus for that purpose the point positions are transformed by a deformation matrix before the algorithm. After processing they are transformed back by the inverse matrix. The decision if the line segment $AB$ crosses the other $CD$ is done by comparing signature of scalar products. We compare signatures of scalar products of a vector perpendicular to $AB$ with $AC$ and the same perpendicular vector to $AB$ with $AD$. If they have different signatures the points $C$ and $D$ lay on the opposite sides of the line segment $AB$ and may cross. The same is done with a vector perpendicular to $CD$ and vectors $CA$,$CB$. If the two corresponding pairs of signatures match, the line segment crosses the other one.

After making triangulation net the corners of the triangles, where the position of the measured current time series lays in, have to be found. It is done also by comparing signatures. The right triangle has to satisfy that each of its corners lays on the same side of the line segment made of the other corners as the position of the measured current time series.

Then a transformation matrix which transforms a triangle to the equilateral triangle with side length of one is counted and the time series position is transformed by the matrix. The relative position in the half-cell is obtained.

# III. Experimental Set-up

The used STM apparatus configuration is basically the same as on figure I.1. The UHV chamber is used with Turbomolecular Varian V 700 pump and Ion pump Vacuum Praha and it is prevacuumed by membrane vacuum pump Alcatel Drytel 31 if the samples or a mechanics in the chamber have been renewed.

The pressure in the chamber is measured by hot-filament ionisation gauge Varian. The whole chamber is air-stabilized by Newport Stabilizer S-2000. And also is placed in the basement of the building for proper suppression of mechanical vibrations.

The samples are held in eight-position revolving holder. The carousel and measuring system are placed on the plate which is hanged on springs with magnetic damping during measurement. The tungsten wire prepared by electrolytic etching in the laboratory is used as the STM tip. The amplifier METEK Signal recovery Model 7270 DSP is used to control piezoceramics and to amplificate of the tunnelling current.

The whole system was designed and developed by the group of thin films. The photo of the used apparatus is in figure III.1

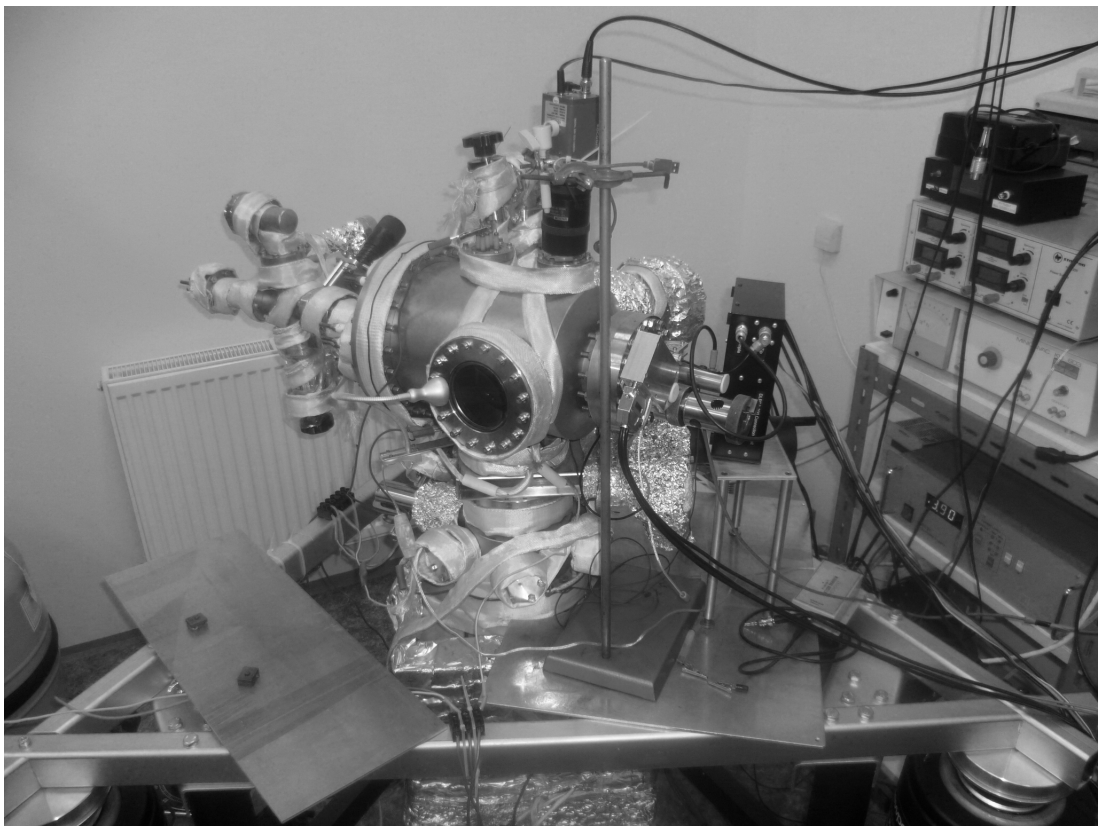

**Figure III.1:** The photo of the STM apparatus

# IV. Experiment

## IV.1 Noise of Tunnelling Current

Separation of the noise from the measured signal is important to be able to analyse the measurement itself. STM is very sensitive device because the tunnelling current is only about nanoamperes or lower. I did analyse the most typical kinds of noises in STM. Examples of them are mechanical interference on the platinum monocrystal caused by bad sample fixing in the holder, flicker noise and shot noise.

### IV.1.1 Mechanical Interference

I measured mechanical noise of the tunnelling current on platinum monocrystal. The reason why it is so visible on the platinum monocrystal is the bad fixing. The monocrystal is fixed in a position by two wires so the whole platinum tends to oscillate. The example of the tunnelling current and its spectral noise density is in figure IV.1.

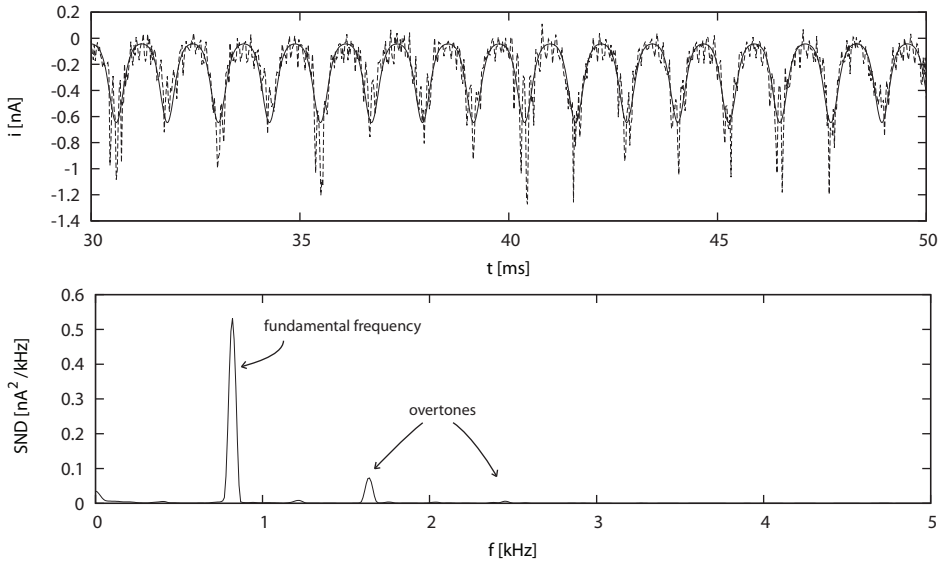


**Figure IV.1:** The fitted (solid line) tunnelling current of mechanical noise on platinum and its spectral noise density

I have fitted the tunnelling current (solid line in figure IV.1) by the function in the programme Gnuplot:

$$f(x) = Ae^{B\sin(Cx+D)} \tag{IV.1}$$

The fitted constants $A, B, C, D$ are:

$$\begin{aligned} A &= (-0.168 \pm 0.008)\ \text{nA} \\ B &= (1.35 \pm 0.06)\ \text{ms}^{-1} \\ C &= (5.140 \pm 0.004) \\ D &= (-4.92 \pm 0.13) \end{aligned}$$

The error estimations are obtained from the programme Gnuplot. We see that the function fits the character of the tunnelling current quite well.

The platinum monocrystal was resoldered after several weeks and the wires which held the monocrystal were shortened. After this modification I measured the oscillation of the platinum monocrystal again. The tunnelling current and spectral noise density are in figure IV.2. The fitted constants are:

$$\begin{aligned} A &= (0.346 \pm 0.010)\ \mathrm{nA} \\ B &= (1.71 \pm 0.03)\ \mathrm{ms}^{-1} \\ C &= (0.15494 \pm 0.00011) \\ D &= (-8.590 \pm 0.019) \end{aligned}$$

We see that the amplitude of oscillations is similar but the measured fundamental frequency is 33 times lower than before the modification of the wires. The problem is that we probably increased the fundamental frequency by shortening the wires so much, that it is higher than the half of sampling frequency. Thus the measured frequency is not correct but it is some high frequency reflected to the lower spectrum.

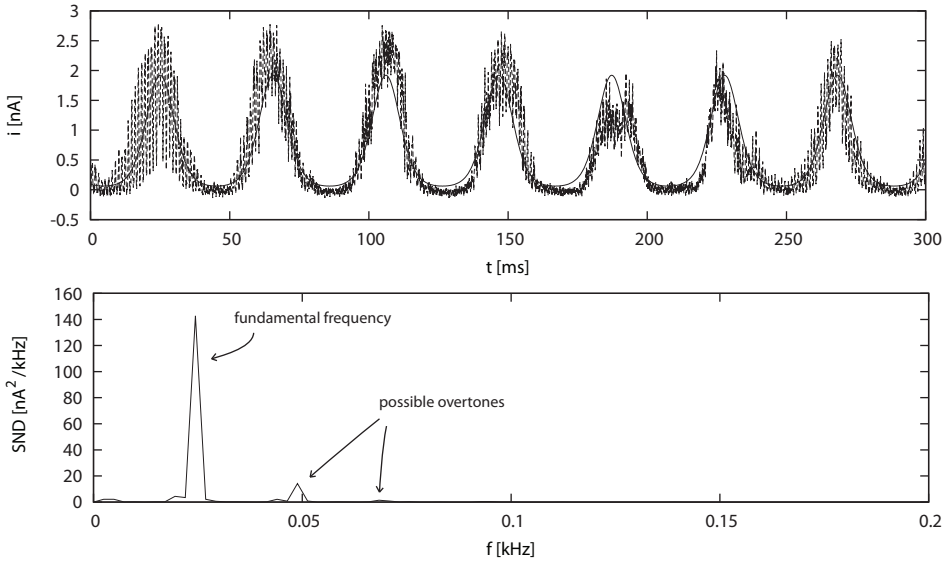


**Figure IV.2:** The fitted (solid line) tunnelling current of mechanical noise on platinum after resoldering of the holder and its spectral noise density

### IV.1.2 Blank Measurement in Half-cell of Si $7 \times 7$

The tunnelling current of an empty half-cell Si $7 \times 7$ was measured. Eight time series of 16 384 points with sampling frequency 10 kHz were acquired and spectral noise densities were evaluated. The average of the measured spectral noise densities is plotted in figure IV.3. There can be seen that there is noise (possible mechanical) with frequency 0.54 kHz (even though the fundamental frequency is suppressed and the largest peak is first overtone at 1.08 kHz) and overtones. The wide peak with frequency 3.37 kHz can be some electrical interference in amplifier or another electronic.

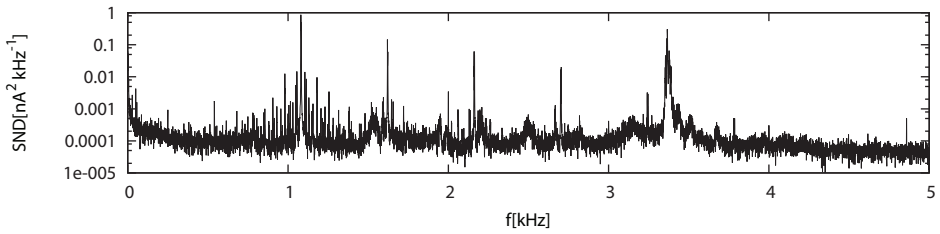


**Figure IV.3:** The spectral noise density of empty half-cells Si $7 \times 7$

Although there is significant interference in the area with higher frequencies we can still analyse atom hopping with time constant bigger than approx. 1 ms.

In figure IV.4 I plotted the detail of spectral noise densities of low frequencies. I fitted it in program Gnuplot with function:

$$f(x) = \frac{A}{x} + B$$

The fitted constant are:

$$\begin{aligned} A &= (1.26 \pm 0.06) \cdot 10^{-5}) \text{ nA}^2 \\ B &= (9.3 \pm 0.8) \cdot 10^{-5}) \text{ nA}^2\text{kHz}^{-1} \end{aligned}$$

The constant $B$ is related to white noise. The shot noise with current 0.3 nA is (equation I.13) approximately $10^{-7}$ nA$^2$kHz$^{-1}$ which is three orders above the fitted constant. The bin size of used A/D converter is 0,003 nA which corresponds to spectral noise density $2 \cdot 10^{-6}$ nA$^2$kHz$^{-1}$. Thus the white noise must be caused by another noise in the used electronics.

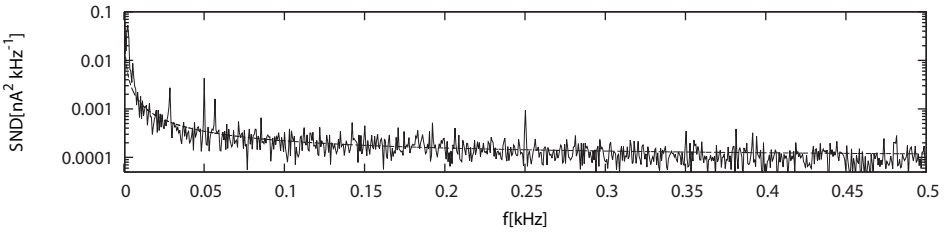


**Figure IV.4:** The fitted detail of the spectral noise density of empty half-cells Si $7 \times 7$

# IV.2 Surface Diffusion on Si Surface

## IV.2.1 Measurement

Diffusion of adsorbed tin on Si (111) $7 \times 7$ surface in UHV $8 \cdot 10^{-9}$ Pa at room temperature was studied. The surface was prepared by the standard procedure of DC annealing and then exposing to evaporation of tin atoms for 2 seconds. The STM tip was enhanced by welding to a wolfram plate and pulling off to form the very tip. After thermal equilibration of the Si sample with the apparatus we started to acquire scanning data.

### IV.2.2 Image Analysis

After compensation of drift of the sample several scans were acquired. The scanning voltage was set to 1.5 or 2.0 V and the tunnelling current to 0.2 or 0.3 nA. There is no visible difference between the individuals set-ups. The scanning speed of acquired images is 77 nm/s. Images were enhanced in the programme Gwydion by applying alignment of rows by median centring and polynomial background subtraction.

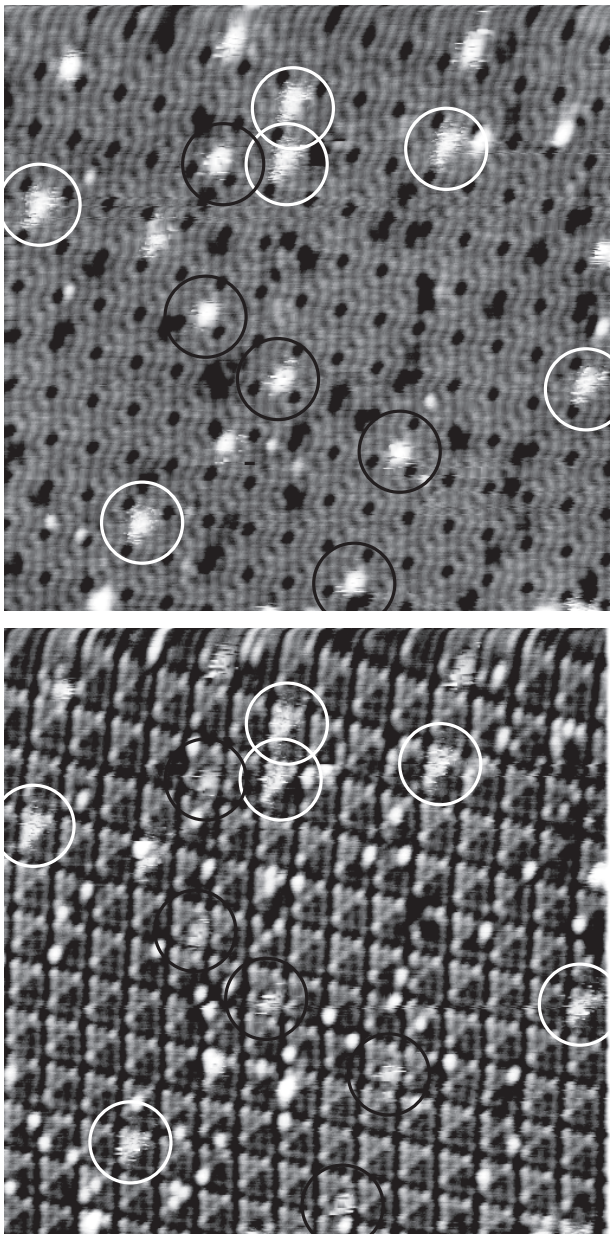

**Figure IV.5:** Scans of adsorbed tin on Si (111) $7\times7$ surface of unoccupied (top image) and occupied (bottom image) states at 2 V and 0.3 nA. Monomers of tin atoms are trapped in faulted/unfaulted half cells and are marked as circles white/ black respectively

In Figure IV.5 there are scanned overviews of the surface with adsorbed tin atoms. The monomers of Sn atom, which are further analysed, are circled, the

other half-cells are with dimers or more atoms. The light, small bulbs which are visible only on the scan of occupied states and on unoccupied seem to be shadows are probably images of other adsorbed atoms or molecules.

### IV.2.3 Observed Types of Half-cell

Different types of imaging half-cells occupied by tin atoms can be seen. By observation and comparing to the study[5], the number of adsorbed Sn atoms in the half-cell was identified. The most common types of half-cells are in figures IV.6 and IV.8. It can be seen that there is a difference between Sn in faulted and unfaulted half-cells. One type of monomer on each un/faulted cell and two fuzzy types of dimer were observed. The Sn atoms appear as fuzzy area. It is because the hopping rate of the Sn atom on the surface is comparable with the scanning speed.

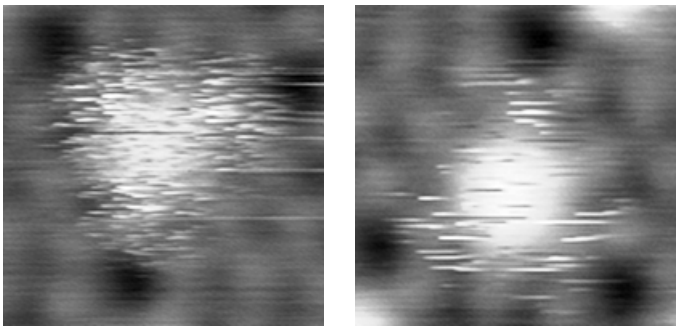

faulted half-cell unfaulted half-cell

**Figure IV.6:** A monomer of a tin atom in half-cells

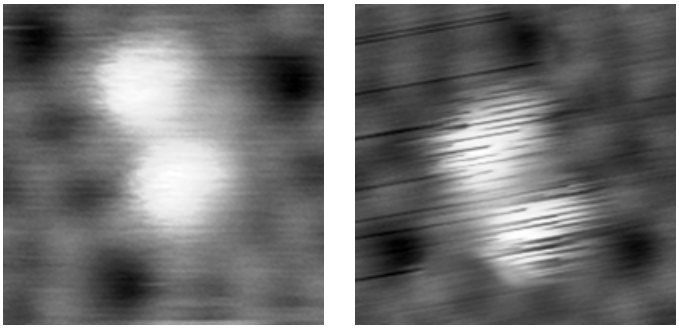

faulted half-cell unfaulted half-cell

**Figure IV.7:** A dimer of tin, type A, in half-cells

From the scan we see that the monomer has a different time constant of hopping in the center and in the corners (More visible on unfaulted half-cell). Also the center of the half-cell is brighter thus that indicates lower energy potential in the center.

The dimers can occur in two types of the fuzzy half-cell - type A and B. In the type A the atoms are situated further at opposite sides of the triangle. In the type B the atoms seem to be close to each other at one side of the triangle.

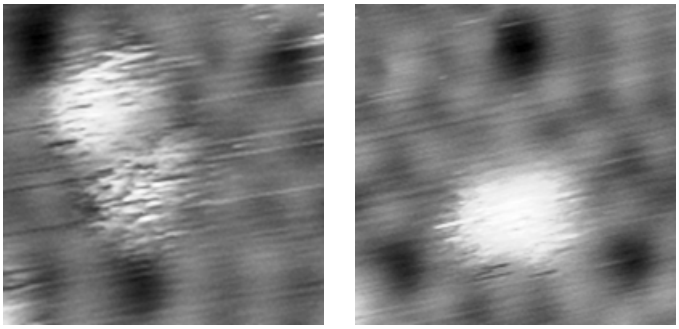

faulted half-cell unfaulted half-cell

**Figure IV.8:** A dimer of tin, type B, in half-cells

We assume that the observed types of the half-cell are dimers because they do not have rotational symmetry and have reflection symmetry. Thus there have to be even number of Sn atoms. The probability of four and higher number of Sn atoms in one half-cell is low (assuming minor Sn-Sn interaction to Sn-surface interaction and low dose of the evaporated tin on the surface). Thus the observed types of the half-cell are most likely dimers.

### IV.2.4 Current Fluctuation Analysis

The time series of the tunnelling current in half-cells were measured. Measurement was made with the STM tip held in the place and acquisition of 16 384 points of the tunnelling current with the time interval 0.1 ms. The tunnelling currents 0.2 nA and 0.3 nA were used. Time series were thereafter analysed. Considering no difference between 0.2 nA and 0.3 nA the series are analysed together. In some positions the current had obvious two-and-more-level character. The multi-level character of the time series is caused by the large radius of the very tip which can thus "feel" the Sn atom in more than one different position.

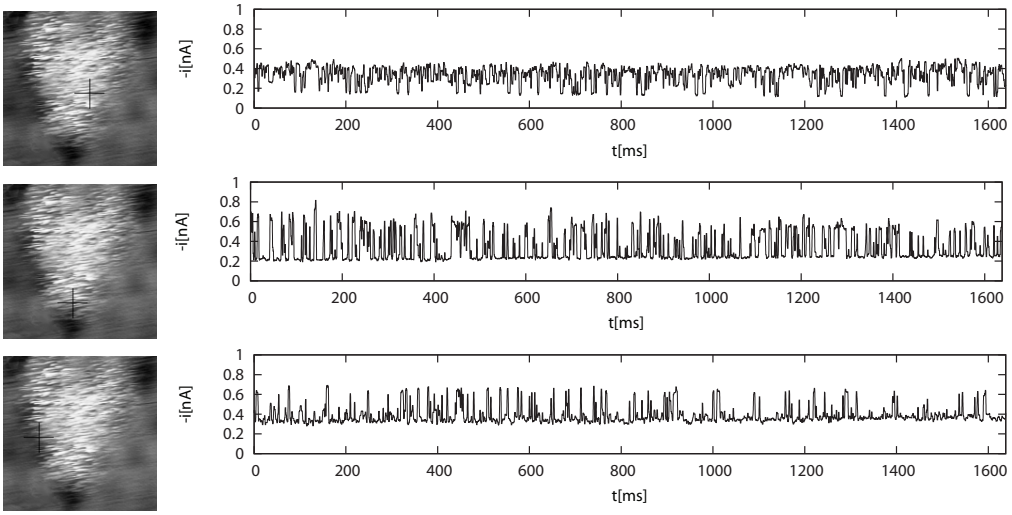


**Figure IV.9:** Examples of the measured tunnelling current in different positions in the faulted half-cell

The time series were post-processed and analysed. Higher frequencies than 1 kHz were cut off by using Fourier transform. The bi-level character was analysed using the algorithms from section II.4. Relative positions in the half-cell were evaluated.

The measured time series were sorted by the type of the half-cell. In figure IV.9 I show examples of acquired data of a monomer in the faulted half-cell in different positions, in figure IV.10 examples of a monomer in unfaulted half-cell.

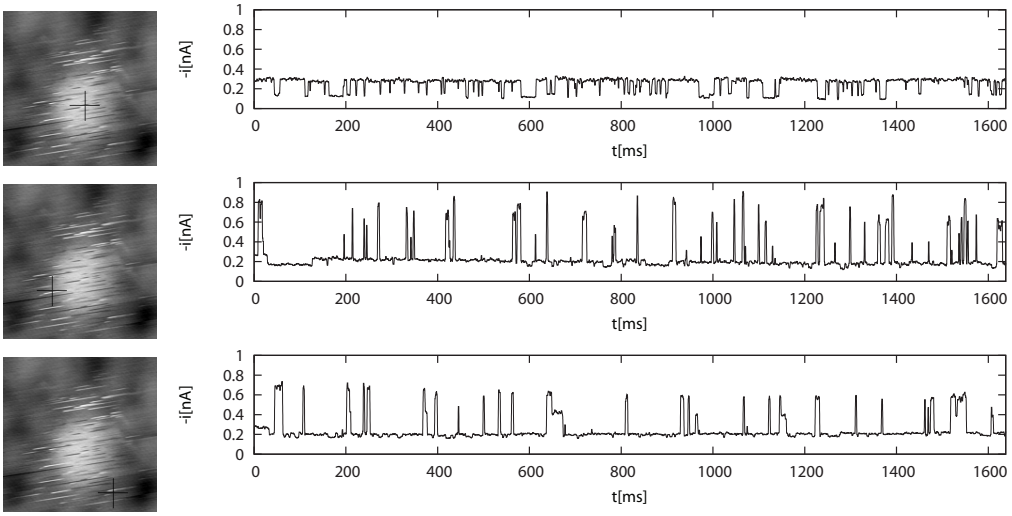


**Figure IV.10:** Examples of the measured tunnelling current in different positions in the unfaulted half-cell

The mean time of Sn atom being in an adsorption position nearest to the tip were evaluated by fitting of a cumulative distribution of duration of the Sn staying in high level of the current (equation II.13). Also the duration of high level of the current comparing to the duration of the whole time series in percent was determined. There were analysed about 90 time series in un/faulted half-cells each and the results were plotted - figures IV.11 and IV.12.

We can see that there is a strong difference between unfaulted and faulted half-cells. In the unfaulted half-cell the Sn atoms were registered in the center where they stay for about 85% of time which corresponds to the scanned image of the half-cell. The hopping among adsorption positions around center is at room temperature so fast that we are not able to measure it. Thus we can measure only hopping between an adsorption position in the center and some in the corner. The preferred position in the center can be also seen in figure IV.13

In the faulted half-cell the situation is quite different. The Sn atom prefers center positions less. In figure IV.14 there is plotted the dependence of residence time on the relative distance to the center of the half-cell from which we see that Sn atom stays in the center longer but in comparison to the figure IV.13 a clear division does not exist. The Sn atom stays in the corner approximately 27% of time.

By averaging fitted mean life times of Sn under the tip in faulted half-cell we get the typical time constant:

$$\tau_f = (1.1 \pm 0.6)\ \text{ms}$$

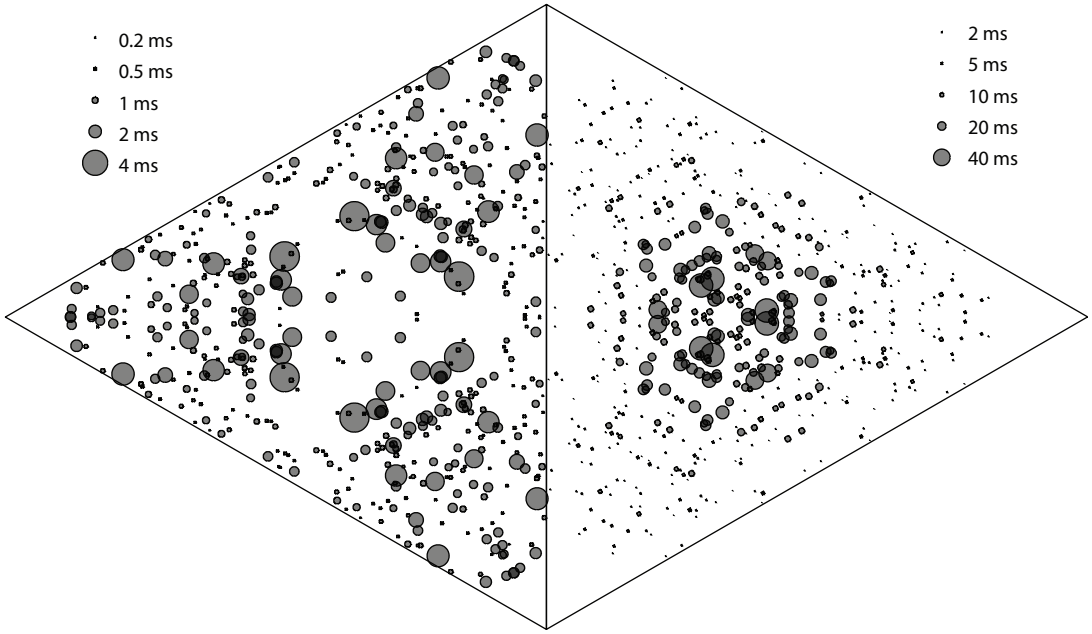


**Figure IV.11:** Map of mean life time of a Sn atom in the adsorption position nearest to the tip. Three-fold symmetry and reflection is used.

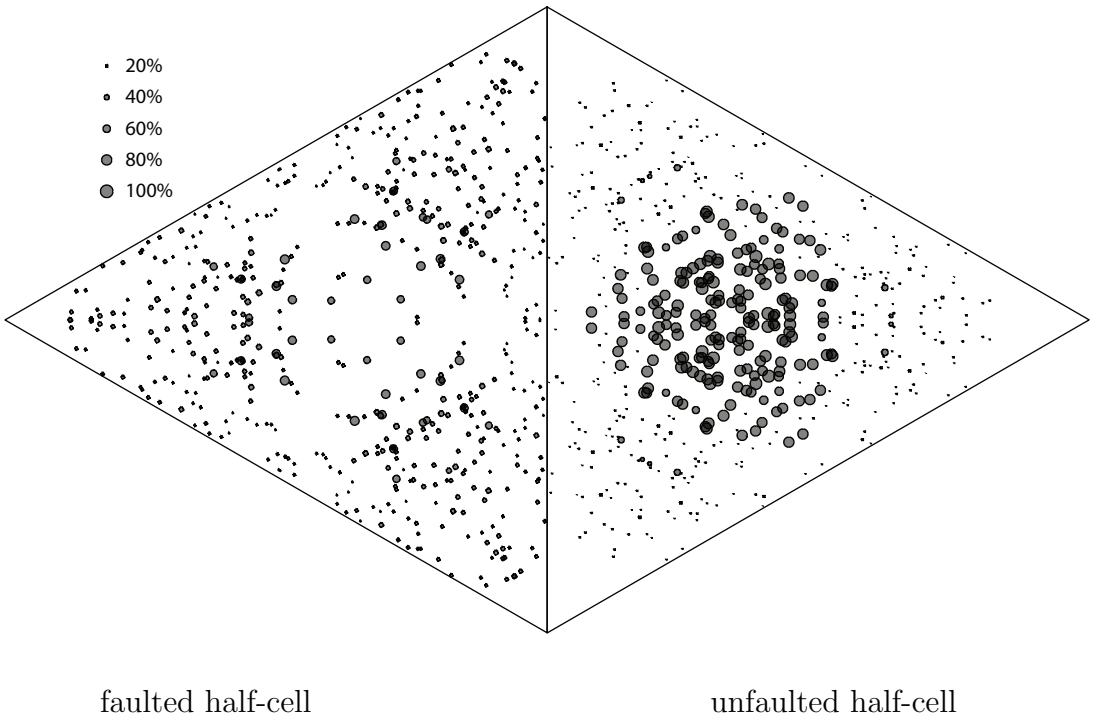


**Figure IV.12:** Map of residence time of a Sn atom in the adsorption position nearest to the tip in percent. Three-fold symmetry and reflection is used.

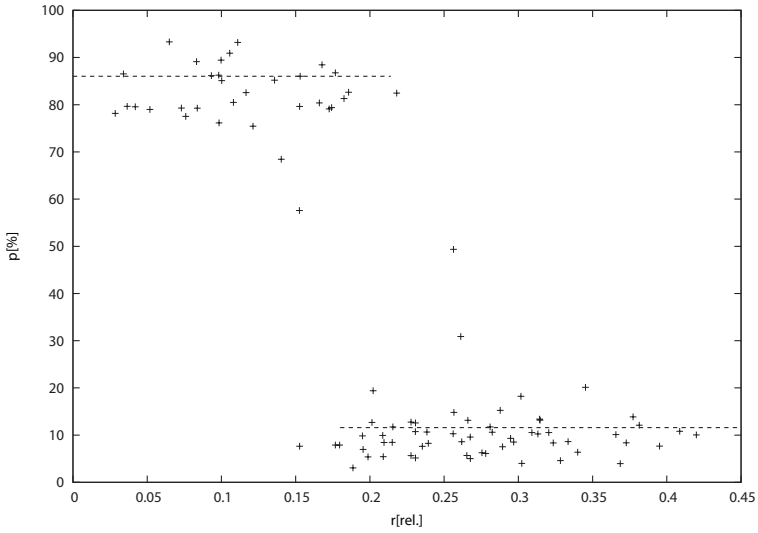


**Figure IV.13:** Dependence of the residence time of Sn atoms in the adsorption position nearest to the tip in percent on the relative distance to the center of the unfaulted half-cell with its side length equal to 1.

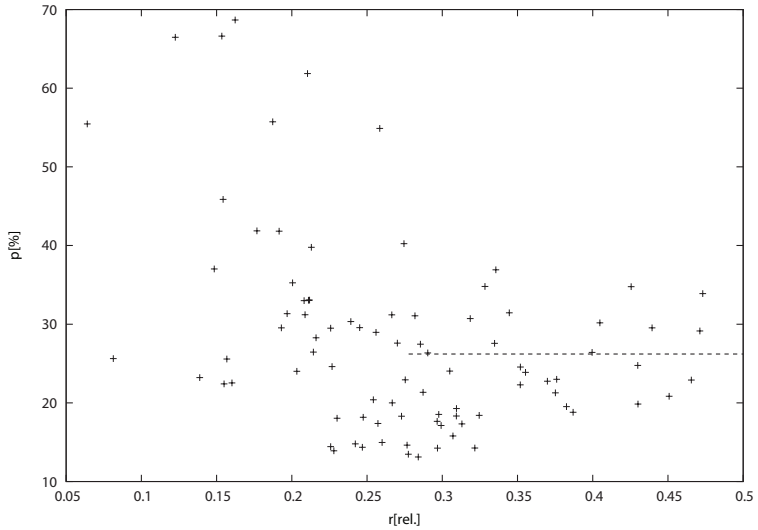


**Figure IV.14:** Dependence of the residence time of Sn atoms in the adsorption position nearest to the tip in percent on the relative distance to the center of the faulted half-cell with its side length equal to 1.

In the unfaulted half-cell, the mean life-time of Sn being in the center of the cell is:

$$\tau_{u,center} = (19.5 \pm 7.4)\ \text{ms}$$

And in the corner:

$$\tau_{u,corner} = (3.5 \pm 2.0)\ \text{ms}$$

Fluctuations of Sn atom were also measured in the unfaulted half-cell with the dimer type A. The character of fluctuations of tunnelling current measured in this type of the half-cell is that there exists only bi-level time series. That is probably because two Sn atoms are bound to each other and thus move like a compound in only two positions. Hopping to another position is unlikely according to the measured tunnelling current. In figure IV.15 there is an example of the measured current. The residence times of high level of the current and low level are 50%. Thus the two possible positions of Sn dimer have to be equivalent.

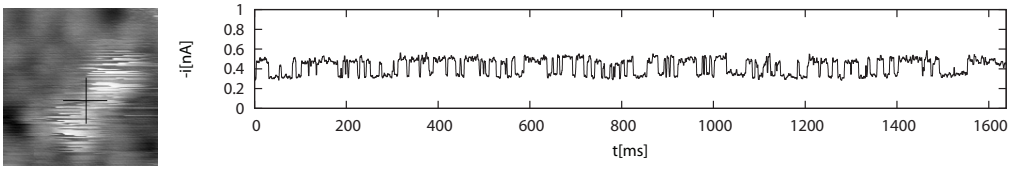


**Figure IV.15:** Examples of measured tunnelling current of dimer type A in the unfaulted half-cell

The average mean life is:

$$\tau_{u,dimer} = (13 \pm 8)\ \text{ms}$$

The other types of Sn dimers do not have specific bi-level fluctuation of the tunnelling current.

# V. Discussion

The resolution of image analysis highly depends on properties of the scanning tip. Three most common undesirable effects at STM measurements are: the creep, the multiple tip and thermal drift. The creep of piezoceramics, which control the tip position, usually occurs when the voltage on the piezoceramics is suddenly changed. The scanned area is shifted and the image is distorted because the delay between the change of voltage and the response of the piezoceramics. The large change of voltage on piezoceramics occurs when the tip jumps from the end of the scanned image to the start of the new one. Thus first rows of the scanned image can be distorted.

The tip can also be multiple. If so, it can be seen on the scanned images that some objects are there more than one times and their positions are in a place where they should not be. Finally, the thermal drift is caused by temperature gradient in the STM measuring head and different temperature expansion coefficients of various materials used. Parts of the apparatus tend to equilibrate with the rest and thus they move in some direction. The thermal drift causes changing of the angles of the half-cell triangles of Si $7 \times 7$.

Those three phenomena contribute firstly to the deviation of the measured position of the tunnelling current time series and secondly to the measured time series themselves. The creep contributes to the error of estimation of the position of the time series at the beginning of the scanned image. The multiple tip smears the objects on the image. The last one - the thermal drift - can be corrected manually and if the motion of the tip is uniform, the contribution to error of the position can be removed completely.

The influence of the multiple tip on the measured time series of the tunnelling current is that the current is captured from multiple positions which is undesirable. The thermal drift in the $x$ and $y$ axis causes that the tip moves above the sample and thus the tunnelling current is not captured from the same position. The motion in $z$-direction cause increasing or decreasing absolute value of the tunnelling current in time.

In the experiments the creep was reduced by measuring with the almost undeflected (with minimal positive and negative voltage) tip where it is not so sensitive to occurrence of the creep. The multiplicity of the tip was corrected if needed by the visual analysis of the scanned images. Finally, the thermal drift was reduced by manual set-up of the motion of the tip but it could not be eliminated completely thus it caused the major contribution to deviation of the measurement.

We suggested that the possible resolution of the tip position can be distinguished if the time series is measured in the center of the half-cell or if it is measured in the corner. For better accuracy the better equipment has to be used or settings of experiment (voltage, scanning speed, tunnelling current, etc.) have to be optimised.

We assume that the presence of the tip and its voltage bias and the tunnelling current do not influence the experiment, mainly the mean life times of the rest of the Sn atoms in the adsorption position. This assumption do not have to be satisfied. Comparing measured data with the tunnelling current 0.2 nA and 0.3 nA we can say that it does not differentiate thus the assumption is satisfied.

The measured time series of the tunnelling current should be measured in static position on the sample for very long time so that we are able to catch enough events of the Sn hops. However, the duration of the measurement is limited because of the previously discussed thermal drift. Thus the number of events, which are in usual time series about tens to a hundred, limited the accuracy of evaluation of the mean life time. The mean life time can be precised by performing more measurement in the same position of the half-cell. However, because of the method of the measurement it is really hard to take the time series in the same position. A better method would be the automated measurement using on-line tracing of the scanned image: mapping the positions of half-cells and acquisition of time series of the tunnelling current in the exact relative position in the half-cell.

About 1000 of time series were taken and evaluated. Hence the automatic algorithmic evaluation was used. But the used algorithms do not have to be optimal. For example the bi-level tresholding neglects the fact that the measured time series of the tunnelling current can be multi-level. Also the algorithm does not count with the fact that the measured time series do not have to be ideal. The tunnelling current can increase (decrease in time). There can be the interference of the tunnelling current from the unknown source. Those causes of errors can be suppressed by optimization of the used algorithms.

Finally because the interference in higher frequencies IV.1.2 the tunnelling current is filtered by Fourier transform thus faster events ($< 1$ ms) can not be recognized.

# Conclusion

The fluctuation of Sn hoping on Si (111) $7 \times 7$ is studied in the thesis. The image analysis of Sn on Si surface scans was done and types of the smallest Sn objects on the surface were classified. The single Sn atom moves in the unfaulted and the faulted half-cell of Si surface differently. In the faulted half-cell, adsorption positions in the center are not so preferred as in the unfaulted half-cell. The average time constant for hopping of the Sn atom was evaluated for the faulted half-cell as:

$$\tau_f = (1.1 \pm 0.6)\ \text{ms}$$

In the unfaulted half-cell the Sn atom moves among adsorption positions in the center of the half-cell with probability 85%. The mean lifetime of Sn staying in the center was determined as:

$$\tau_{u,center} = (19.5 \pm 7.4)\ \text{ms}$$

And in the corner:

$$\tau_{u,corner} = (3.5 \pm 2.0)\ \text{ms}$$

The results were obtained from about 1000 acquisitions of tunnelling current time series in different positions and types of fuzzy half-cell. The time series were classified according to the type of the half-cell, relative positions of the measured time series in the half-cell were determined, the bi-level fitting of the tunnelling current was performed and the average duration of the high level of the tunnelling current were evaluated.

Also fluctuations of the tunnelling current were studied. Mechanic oscillations on platinum monocrystal and the blank measurement of the tunnelling current in empty half-cells were analysed.

All tasks apart from low temperature measurement, which could not be done due to unavailability of necessary measuring equipment, were accomplished.

The research can continue with the low temperature experiments and attempt of increased accuracy of positions of the tunnelling current time series.

# Bibliography


[1] AMBRÓZY, A. *Electronic Noise*. Budapešť: Akadémiai Kiadó, 1982.

[2] CEJNAR, P. *A Condensed Course of Quantum Mechanics*. Prague: Karolinum, 2013.

[3] CHANG, C.M., WEI, C.M. Diffusion of an adsorbed Si atom on the Si(111)-(7 × 7). *Physical Review B*. 2003, **67**,033309.

[4] CHEN, C. J.: *Introduction to Scanning Tunneling Microscopy*. USA: Oxford University Press, 1993.

[5] CUSTANCE, O., BRIHUEGA, I., GÓMEZ-RODRÍGUEZ, J.M., BARÓ, A.M. Initial stages of Sn adsorption on Si(111)-(7 × 7). *Surface Science*. 2001, **482-485**, 1406-1412.

[6] CUSTANCE, O., BROCHARD, S., BRIHUEGA, I., ARTACHO, E., SOLER, J.M., BARÓ, A.M., GÓMEZ-RODRÍGUEZ, J.M. Single adatom adsorption and diffusion on Si(111)-(7 × 7) surfaces: Scanning tunneling microscopy and first-principles calculations. *Physical Review B*. 2003, **67**,235410.

[7] HAHNE, S., IKONOMOV, J., SOKOLOWSKI, M., MAASS, P. Determining molecule diffusion coefficients on surfaces from locally fixed probe: On the analysis of signal fluctuations. *physical Review B*. 2013, **87**,085409.

[8] HWANG,I., LO, R.,TSONG, T.T. Site Hopping of Single Chemisorbed Oxygen Molecules on Si(111)-(7 × 7). *Physical Review Letters*. 1997, **78**(25).

[9] JOHNSON, J.B. Thermal Agitation of Electricity in Conductors *Physical Review*, 1928, **32**,97-109.

[10] KEHUI, W. ,FUJIKAWA, Y., NAGAO, T., HASEGAWA, Y., NAKAYAMA, K.S., XUE, Q.K., WANG, E.G., BRIERE, T.,KUMAR, V., KAWAZOE, Y., ZHANG, S.B., SAKURAI, T. Na Adsorption on the Si(111)-(7 × 7) Surface: From Two-Dimensional Gas to Nanocluster Array. *Physical Review Letters*. 2003, **91**(12).

[11] LAGOUTE, J., ZAMBELLI, T., MARTIN, S. GAUTHIER, S. Spatial Repartition of Current Fluctuations in a Scanning Tunneling Microscope. *Image Anal Stereol*. 2001, **20**, 175-179.

[12] LIAO, P., CHEN, T., CHUNG, P. A Fast Algorithm for Multilevel Tresholding. *Journal of Information Science and Engineering*. 2001, **17**,713-727.

[13] LIN, X.F., CHIZHOV, I., MAI, H.A., WILLIS, R.F. Interaction of Sn atoms with intrinsic dangling-bond states of Si(111)-(7 × 7) *Surface Science*. 1996, **366**,51-59.

[14] LO, R., HWANG, I., HO, M., TSONG, T.T. Diffusion of Single Hydrogen Atoms on Si(111)-(7 × 7) Surfaces. *Physical Review Letters*. 1998, **80**(25).

[15] LOZANO, M.L., TRINGIDES, M.C. Surface Diffusion Measurements from STM Tunneling Current Fluctuations. *Europhysics Letters*. 1995, **30**(9), 537-542.

[16] MAEDA, K., SUGITA, S., KURITA, H., UOTA, M., UCHIDA, S., HINOMARE, M., MERA, Y. Spatial variation of 1/f current noise in scanning tunneling microscopes. *Journal of Vacuum Science & Technology B*. 1994, **12**,2140.

[17] MAKOTO, I.:*Si(111) surface.*[online].[cit. 21.5.2014]. Dostupné z: http://www.geocities.jp/mitoh6/index.html

[18] MANASSEN, Y., BALATSKY, A.V. 1/f Spin Noise and a Single Spin Detection with STM. *Israel Journal of Chemistry*. 2004, **44**(4),401-408

[19] MIROV, V.L.: *Fundamentals of Scanning Probe Microscopy* Nizhniy Novgorod: 2004.

[20] PROAKIS, J. G., MANOLAKIS, D. G.: *Digital Signal Processing: Principles, algorithms, and applications.* Upper Saddle River: Prentice Hall, 2007.

[21] SUGITA, S., MERA, Y., MAEDA, K. Origin of low frequency noise and 1/f flucuations of tunneling current in scanning tunneling microscopes. *Journal of Applied Physics*.1993, **79**(4166).

[22] ŠIŠTÍK, L., ONČÁK, M., SLAVÍČEK, P.: *Stručný úvod do teoretické a počítačové chemie.* [online]. [cit. 5.4.2014]. Dostupné z: http://www.vscht.cz/fch/cz/pomucky/Prirucka_TeorChem.pdf

[23] TAKAYANAGI, K., TANISHIRO, Y., TAKAHASHI, S., TAKAHASHI, M. Structure analysis of Si(111)-7 $\times$ 7 Reconstructed Surface by Transmission Electron Diffraction *Surface Science*. 1895, **164**, 367-392.

[24] WANG, K., CHEN, G., ZHANG, C., LOY, M.M.T., XIAO, X. Intermixing of Interbasin Diffusion of a Single Ag Atom on Si(111)-(7$\times$7. *Physical Review Letter*. 2008, **101**, 266107

[25] WANG, K., ZHANG, C., LOY, M.M.T., XIAO, X. Time-Dependent Tunnaling Spectroscopy for Studying Surface Diffusion Confined in Nanostructures. *Physical Review Letters*. 2005, **94**, 036103